

NASA TECHNICAL NOTE



NASA TN D-2043

c.f

NASA TN D-2043

TOAN COPY: RETL
AFWL (WLL-
KIRTLAND AFB, N



**CALCULATED RADIO ATTENUATION
DUE TO PLASMA SHEATH ON
HYPERSONIC BLUNT-NOSED CONE**

by John S. Evans and Paul W. Huber

*Langley Research Center
Langley Station, Hampton, Va.*



TECHNICAL NOTE D-2043

CALCULATED RADIO ATTENUATION DUE TO PLASMA SHEATH ON
HYPERSONIC BLUNT-NOSED CONE

By John S. Evans and Paul W. Huber

Langley Research Center
Langley Station, Hampton, Va.

NATIONAL AERONAUTICS AND SPACE ADMINISTRATION

CALCULATED RADIO ATTENUATION DUE TO PLASMA SHEATH ON
HYPERSONIC BLUNT-NOSED CONE

By John S. Evans and Paul W. Huber

SUMMARY

Electron concentration and collision frequency were evaluated at several axial flow stations along a blunt-nosed 9° half-angle cone flying at zero angle of attack, 17,700 ft/sec, and 170,000-foot altitude. These conditions were chosen to correspond to those for the maximum observed attenuation during the flight of the RAM A1 vehicle. Equilibrium, frozen, and finite-rate flow assumptions were made about both chemical and ionic processes. Boundary-layer concepts were applied to modify the results near the body. Signal attenuation at 240 mc was computed by numerical integration through the plasma layer of the propagation equation for electromagnetic radiation. The propagation model was a monochromatic plane wave normally incident on a plane-parallel plasma in which electron concentration and collision frequency varied only in the propagation direction.

INTRODUCTION

The ionized layer around a space vehicle during reentry strongly attenuates radio signals and therefore often breaks communication links with the ground. The importance of the problem has been recognized for some time (ref. 1) and many papers have been written which pertain to it in one way or another.

Most of the experimental flight data on signal attenuation have come from telemeter records of flights which had objectives other than the study of communications problems. As a result, these data commonly show little more than that the signal blacked out during a certain part of the trajectory. The RAM (Radio Attenuation Measurement) project at the Langley Research Center has obtained better data than those by flying blunt-nosed slender bodies designed to give measurable attenuation without signal blackout and to give quantitative information about the amount of signal attenuation, the effect of the plasma on the antenna, the plasma properties, and the attitude, altitude, and velocity of the vehicle. Reference 2 reports the results of the RAM A1 flight.

A good theoretical understanding of the signal attenuation problem is necessary not only for intelligent interpretation of flight data but also for advancement of the art of designing future communications systems. There are two basic parts to the theoretical problem: the specification of the plasma parameters, and the calculation of the effect of the plasma on the electromagnetic wave which passes through it.

For a hypersonic vehicle the first part of the problem involves a calculation of the real-gas flow field around the body in sufficient detail to give the electron concentration and collision frequency profiles through the shock layer at the body stations corresponding to antenna locations. The profiles obtained depend strongly upon whether chemical and ionic reaction rates are fast or slow relative to flow time over the body. Important differences in the profiles are also produced by allowing for a boundary layer near the surface. No calculations for complete nonequilibrium flow fields including boundary layer have appeared in the literature. However, several useful calculations for inviscid, real-gas, blunt-body flow fields have been reported. Typical papers from this group are reference 3, which reports thermodynamic and flow properties for equilibrium air in inviscid flow over a blunted 90° half-angle cone, and references 4, 5, and 6, which report the calculated finite-rate variation of electron concentration along streamlines in inviscid flow over some other blunt bodies. Calculations for chemically reacting boundary layers have been reported in references 7, 8, and 9.

In order to test the effect on calculated radio signal attenuation of various assumptions about the nature of the flow without a large expenditure of effort on computations, new methods have been developed, and are described herein, by means of which real-gas, nonequilibrium flow fields, including boundary-layer effects, can be specified with reasonable confidence from normalized shock-layer profiles derived from published results of detailed equilibrium inviscid calculations over a wide range of flight conditions.

The second basic part of the theoretical problem requires the solution of the propagation equation for electromagnetic waves through a region in which the conductivity of the medium is complex, variable, and characterized by gradients which are too steep to permit WKB solutions (ref. 10) to be used. Analytic solutions valid for steep electron concentration gradients are available for special profiles (ref. 11), but these do not offer the flexibility necessary for general use. A unique method has been devised for accomplishing numerical integration of the propagation equations. Although numerical integration of these equations through the plasma in the direction of propagation is not possible because of the contribution of reflection to the initial boundary conditions, the equations can be integrated in the reverse direction if the transmitted electric vector is normalized to unit amplitude and zero phase angle. Solutions of this kind are used herein, and the method has been checked by comparison of special calculations to published results for profiles which lead to analytic solutions (ref. 12). Subsequent to the development and first publication (ref. 13) of the foregoing method (for normal incidence only), a paper (ref. 14) appeared which described the independent development of essentially the same approach to the problem of solving the propagation equations for arbitrary angles of incidence. A computer program for arbitrary angles of incidence was already in operation at the Langley Research Center when reference 14 came to the authors' attention, but the results were not published until some time later (ref. 12).

A brief preliminary presentation of results was given at the Second Plasma Sheath Symposium (ref. 13). Reference 13 also includes a comparison of calculated and observed attenuation during the flight of the RAM A1 vehicle.

SYMBOLS

C_p pressure coefficient, $\frac{p - p_\infty}{q_\infty}$

D_n nose diameter, 5.08 cm for RAM A vehicle

E electric field intensity, volts/meter

E_R electric field intensity reflected by plasma layer

E_T transmitted electric field intensity

$$\bar{E} = \frac{E}{|E_T| e^{i(k_0 \Delta + \phi_b)}}$$

$$\bar{E}_R = \frac{E_R}{|E_T| e^{i(k_0 \Delta + \phi_b)}}$$

e^- electron

f real part of complex number representing E

$$\bar{f} = \frac{f}{|E_T|}$$

g imaginary part of complex number representing E

$$\bar{g} = \frac{g}{|E_T|}$$

$$I = \frac{e^{-i(k_0 \Delta + \phi_b)}}{|E_T|}$$

$$i = \sqrt{-1}$$

k wave number; reaction rate (dimension of wave number is cm^{-1} ; dimension of reaction rate is $\text{cm}^3\text{-molecule}^{-1}\text{-sec}^{-1}$)

N atomic nitrogen

N_2 molecular nitrogen

NO nitric oxide

NO^+ nitric oxide ion

O	atomic oxygen
O ₂	molecular oxygen
p	pressure, atm
\bar{Q}	velocity-averaged effective collision cross section for electrons with neutrals in air, cm ²
q	dynamic pressure, atm
R	universal gas constant
r	radius of body at x/D_n , cm
S	entropy
(SL) _R	signal loss due to reflection, db
(SL) _t	total signal loss, db
s	distance along streamline from shock front, cm
T	temperature, °K
t	time, sec
u	velocity, ft-sec ⁻¹
V	real part of square of k/k_0
W	imaginary part of square of k/k_0
w	mass-flow parameter, slug-sec ⁻¹
x	distance along body axis from stagnation point, cm
y	distance from body along normal to body surface, cm
α	degree of dissociation of air; phase parameter in equations (9) and (12), cm ⁻¹
β	attenuation parameter in equations (9) and (13), cm ⁻¹
γ	ratio of specific heats
Δ	thickness of shock layer measured along y , cm
Δ _n	shock standoff distance at nose, cm
δ	boundary-layer thickness, cm

ν	collision frequency of an electron with neutral particles in air, sec^{-1}
ρ	density, slugs-ft^{-3}
ϕ	phase angle of E relative to phase of E_{0a} , radians
ω	angular signal frequency, radians-sec^{-1}
ω_p	angular plasma frequency, radians-sec^{-1}
$[]$	concentration, particle cm^{-3}
$ $	magnitude of a complex number

Subscripts:

0	medium containing incident and reflected electromagnetic waves
1	plasma portion of wave medium
2	medium containing transmitted electromagnetic waves
a	boundary between medium 0 and medium 1
b	boundary between medium 1 and medium 2
b ℓ e	boundary-layer edge
bs	body streamline (in inviscid flow)
d	dissociation rate of molecules in air
ns	normal shock
o	free-space value
r	recombination rate of electrons in air
s	shock property
s ℓ	standard sea-level conditions
∞	free stream

Flow-field notation:

EQ	flow field in which chemical and ionic reactions are everywhere in equilibrium
EQBL	same as EQ but with boundary-layer corrections to temperature and density

- FD flow field in which chemical reaction rates vanish downstream of freeze point on each streamline
- FDFRBL same as FD but with boundary-layer corrections to temperature, density, and velocity and also with allowance for finite rate recombination of electrons along streamlines
- FS flow field in which chemical and ionic reaction rates vanish downstream of shock wave, but shock is at equilibrium
- SFD same as FD except that $[e^-]$ is in local equilibrium
- SFS same as FS except that $[e^-]$ is in local equilibrium

Prime to a symbol denotes a derivative with respect to y .

FLOW-FIELD CONSIDERATIONS

A schematic diagram of the flow field over the RAM body in flight is given in figure 1. The coordinate system shown is used throughout the paper.

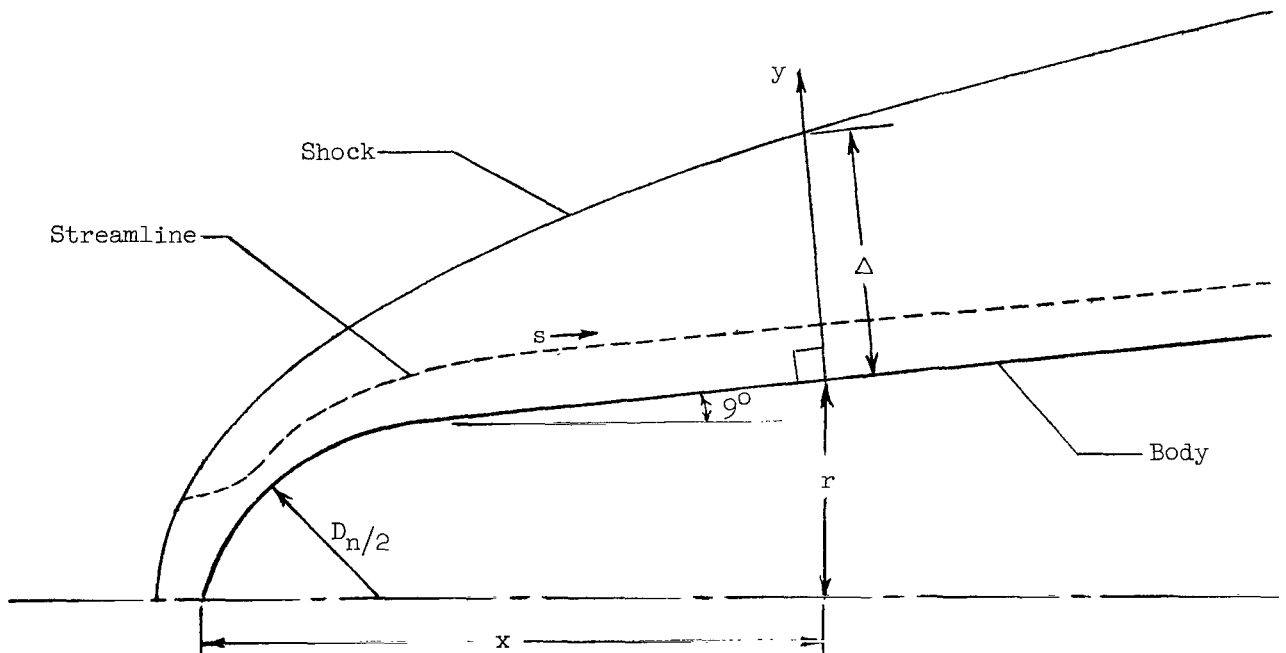


Figure 1.- Flow-field diagram for RAM A vehicle.

The equilibrium inviscid flow-field properties were determined by means of an interpolation technique which adapted numerical flow-field results (ref. 3) for equilibrium inviscid flow over a blunted 90° half-angle cone at selected velocity-altitude points to the velocity and altitude corresponding to peak

In order to use the plots shown in figures 2 and 3, the body and shock values of entropy and pressure under the flight conditions of interest must be specified. It is in the insertion of these boundary values, particularly the body value, that the real-gas effects are reintroduced. This is done as follows: (a) entropy is constant along the body streamline and is equal to the normal shock or stagnation-point value at the nose; (b) entropy along the shock is related to normal shock entropy and to free-stream entropy by means of the normalized plot shown in figure 4; (c) body and shock pressures are related to the normal shock and free-stream pressures by means of the normalized pressure-distribution curves of figure 5.

Figures 4, 5, and 6, like figures 2 and 3, represent the results of reducing real-gas numerical solutions such as those of reference 3. These plots are not as independent of flight conditions as are those of figures 2 and 3. Thus, flight conditions most closely approximating those required were chosen for the preparation of these plots. Figure 6 is a plot of shock-layer thickness along the body in terms of the shock standoff distance at the nose. When this curve is used, the value of the shock standoff distance can be found from the Lighthill equation:

$$\frac{\Delta_n}{D_n} = 0.35 \left(\frac{\rho_\infty}{\rho_{ns}} \right) + 0.002$$

The real-gas flow properties behind the normal shock and for the ambient free stream as functions of altitude and velocity were taken from reference 15.

The interpolation technique which has been described is useful as an expedient means for approximating flow-field properties. It permits reasonably accurate evaluation of equilibrium inviscid flow-field properties over bodies of a given shape for arbitrary values of velocity and altitude over a fairly wide range. It is worth noting that the body values of the flow parameters can be more accurately determined than the shock values and that the flow parameters near the body are those of prime importance to radio-signal-attenuation predictions. The flow properties computed for RAM A1 at the peak attenuation point on its trajectory are summarized in table I. The properties specified are pressure distribution and shock and streamline coordinates.

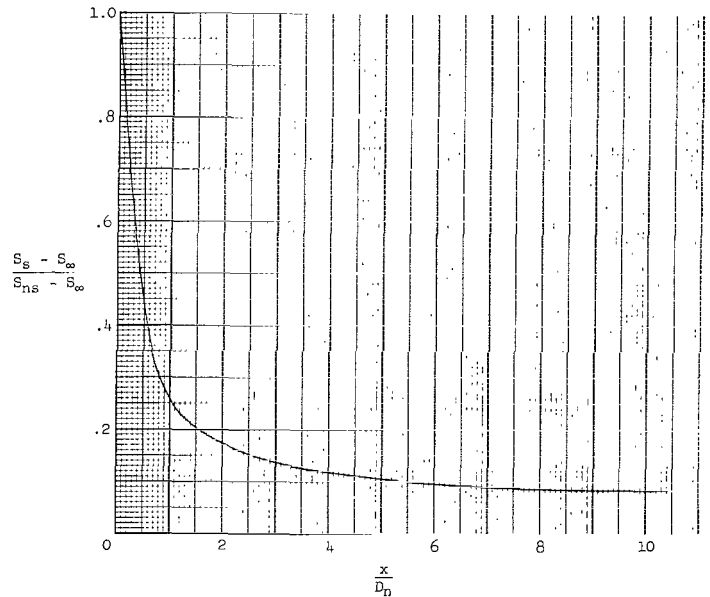


Figure 4.- Entropy distribution along shock in equilibrium inviscid flow over a blunted 9° half-angle cone.

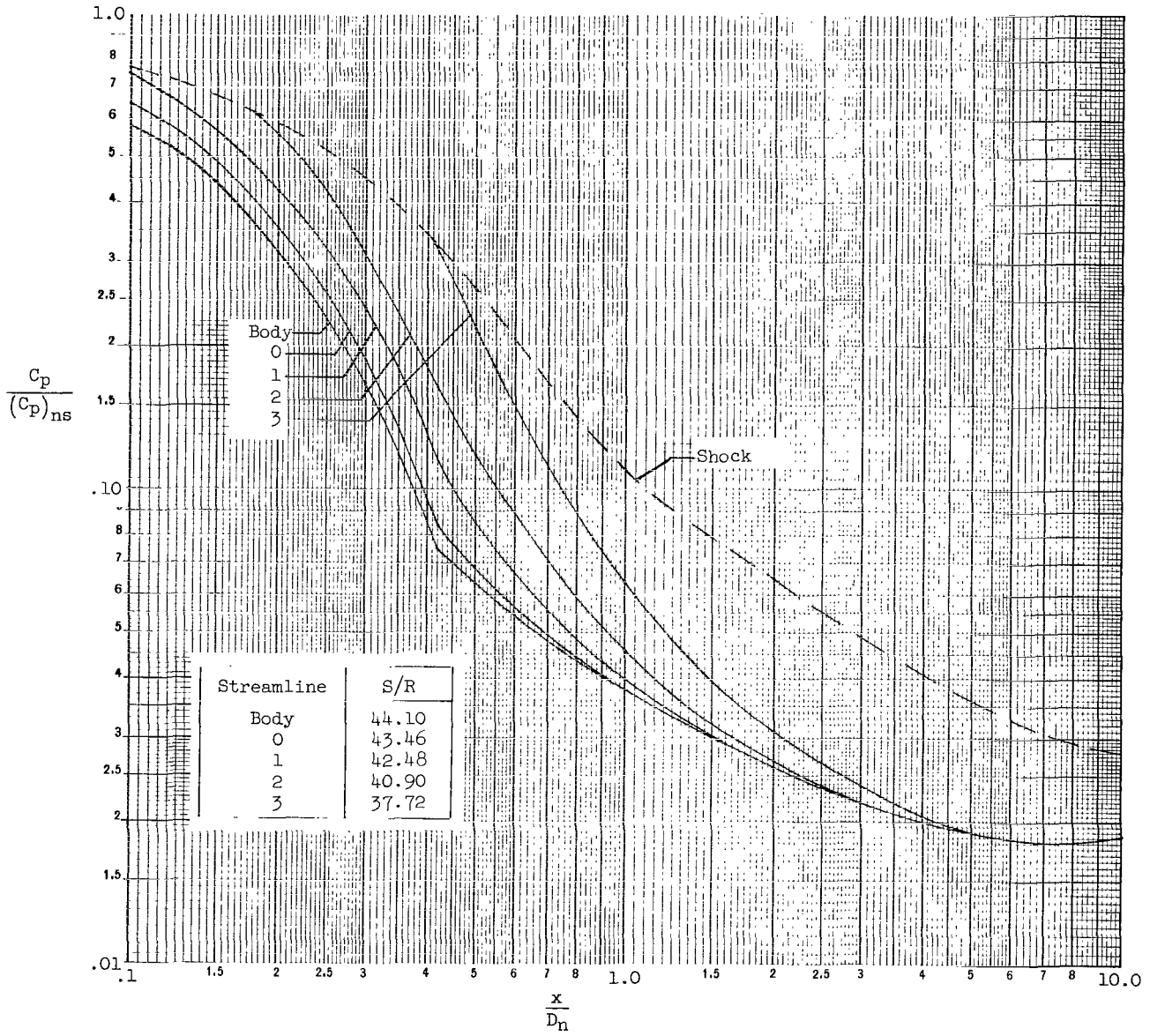


Figure 5.- Pressure distribution along streamlines in equilibrium inviscid flow over a blunted 9° half-angle cone.

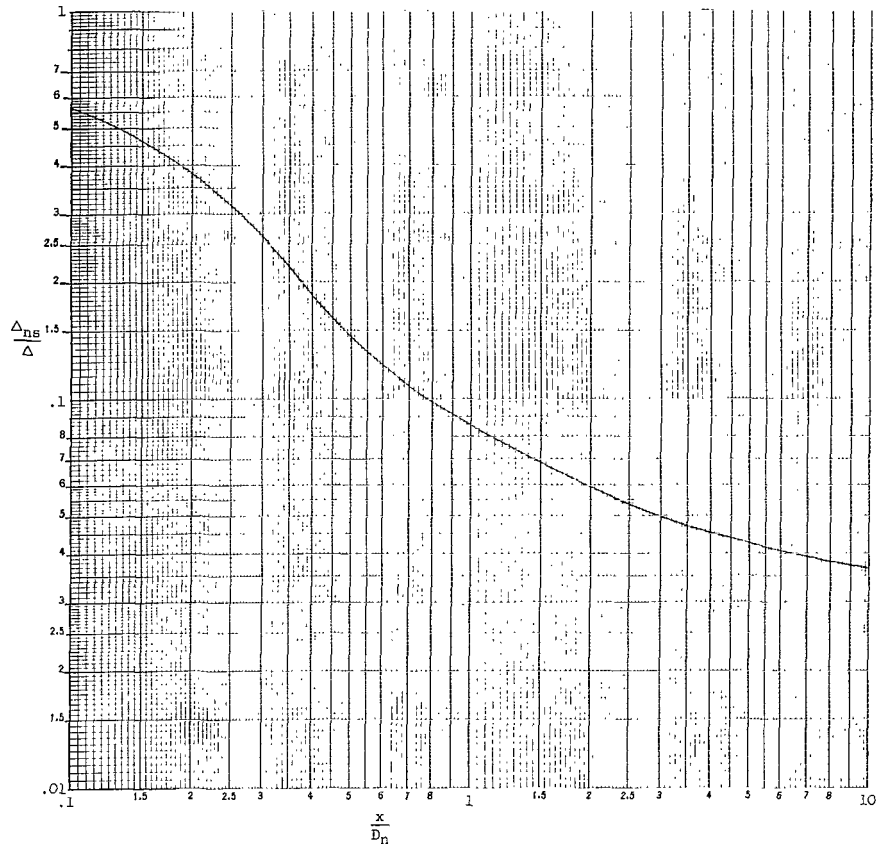


Figure 6.- Shock-layer thickness for inviscid equilibrium flow over a blunted 90° half-angle cone.

Shock coordinates, streamline coordinates, and pressure distributions were used without change for nonequilibrium inviscid as well as equilibrium inviscid flow, since these properties are relatively insensitive to changes in chemical composition for the RAM shape. Temperature, density, and composition for equilibrium inviscid flow were followed along streamlines by using pressure and entropy as inputs to real-air property tabulations. Temperature, velocity, and density for frozen inviscid flow were obtained from isentropic flow relations by using pressure distributions along streamlines and initial conditions at the freeze point as inputs. The specific heats and enthalpies used in the isentropic frozen-flow expansions were computed on the basis of fixed composition as determined at the freeze point. The internal energies of the species were assumed to be in equilibrium with the translational temperature throughout the frozen expansion.

Streamlines entering the boundary layer were followed by using a boundary-layer mass-flow parameter. The boundary-layer thermal properties and velocity distributions were determined by means of the laminar similar solutions treatment for equilibrium boundary layers described in reference 16. The way in which this boundary-layer treatment was adapted for use in frozen flow and also the

TABLE I.- ENTROPY AND PRESSURE ALONG STREAMLINES IN EQUILIBRIUM INVISCID FLOW OVER A

BLUNTED 9° HALF-ANGLE CONE

[Altitude = 170,000 ft; Velocity = 17,700 ft/sec]

(a) Entropy

$$\frac{\Delta s_{ns}}{D_n} = 0.03; \frac{S_\infty}{R} = 31.00; \frac{S_{ns}}{R} = 44.10$$

Streamline	S/R
Body	44.10
0	43.46
1	42.48
2	40.90
3	37.72

(b) Pressure distribution and streamline coordinates

$\frac{x}{D_n}$	Body		0		1		2		3		Shock	
	$\frac{y}{\Delta}$	$\frac{(C_p)_{bs}}{(C_p)_{ns}}$	$\frac{y}{\Delta}$	$\frac{C_p}{(C_p)_{ns}}$	$\frac{y}{\Delta}$	$\frac{C_p}{(C_p)_{ns}}$	$\frac{y}{\Delta}$	$\frac{C_p}{(C_p)_{ns}}$	$\frac{y}{\Delta}$	$\frac{C_p}{(C_p)_{ns}}$	$\frac{\Delta}{D_n}$	$\frac{(C_p)_s}{(C_p)_{ns}}$
0.1	0	0.580	0.355	0.647	0.835	0.750	-----	-----	-----	-----	0.053	0.770
.2	0	.315	.213	.354	.496	.427	0.915	0.561	-----	-----	.079	.588
.3	0	.167	.168	.187	.418	.241	.660	.313	-----	-----	.114	.450
.42	0	.075	.148	.084	.327	.116	.579	.164	0.991	0.320	.172	.325
.5	0	.064	.147	.069	.317	.086	.533	.118	.908	.217	.207	.263
.75	0	.046	.134	.047	.288	.052	.500	.065	.807	.099	.290	.153
1.0	0	.038	.119	.038	.259	.040	.446	.046	.759	.064	.349	.110
2.0	0	.026	.082	.026	.183	.026	.329	.027	.593	.031	.504	.065
3.0	0	.022	.059	.022	.140	.022	.266	.022	.501	.024	.601	.049
4.0	0	.020	.050	.020	.119	.020	.231	.020	.446	.021	.663	.041
5.0	0	.019	.041	.019	.103	.019	.206	.019	.405	.019	.705	.036
7.5	0	.018	.034	.018	.082	.018	.165	.018	.340	.018	.774	.030
10.0	0	.019	.029	.019	.073	.019	.146	.019	.303	.019	.820	.028

method for matching the boundary-layer profile to the shock-layer profile are described later.

As previously stated, the main objective of the study was to compare the effect on predicted radio signal attenuation of several assumptions about the nature of the flow. Three kinds of assumptions were made. First, the thermal state of the air was assumed to be completely determined by the neutral molecules and atoms. For the flight conditions chosen this is a valid approximation for the determination of thermodynamic properties, since the ion concentrations are too small to have an appreciable effect on the thermal properties. Calculations were made for the following limiting conditions: (1) complete chemical equilibrium throughout the flow, and (2) frozen chemistry subsequent to the attainment of complete chemical equilibrium in the shock front. A more realistic calculation was made in which dissociation occurred at a finite rate behind the shock front until a "freeze point" was reached. Typical streamline temperature distributions for these three conditions are shown in figure 7.

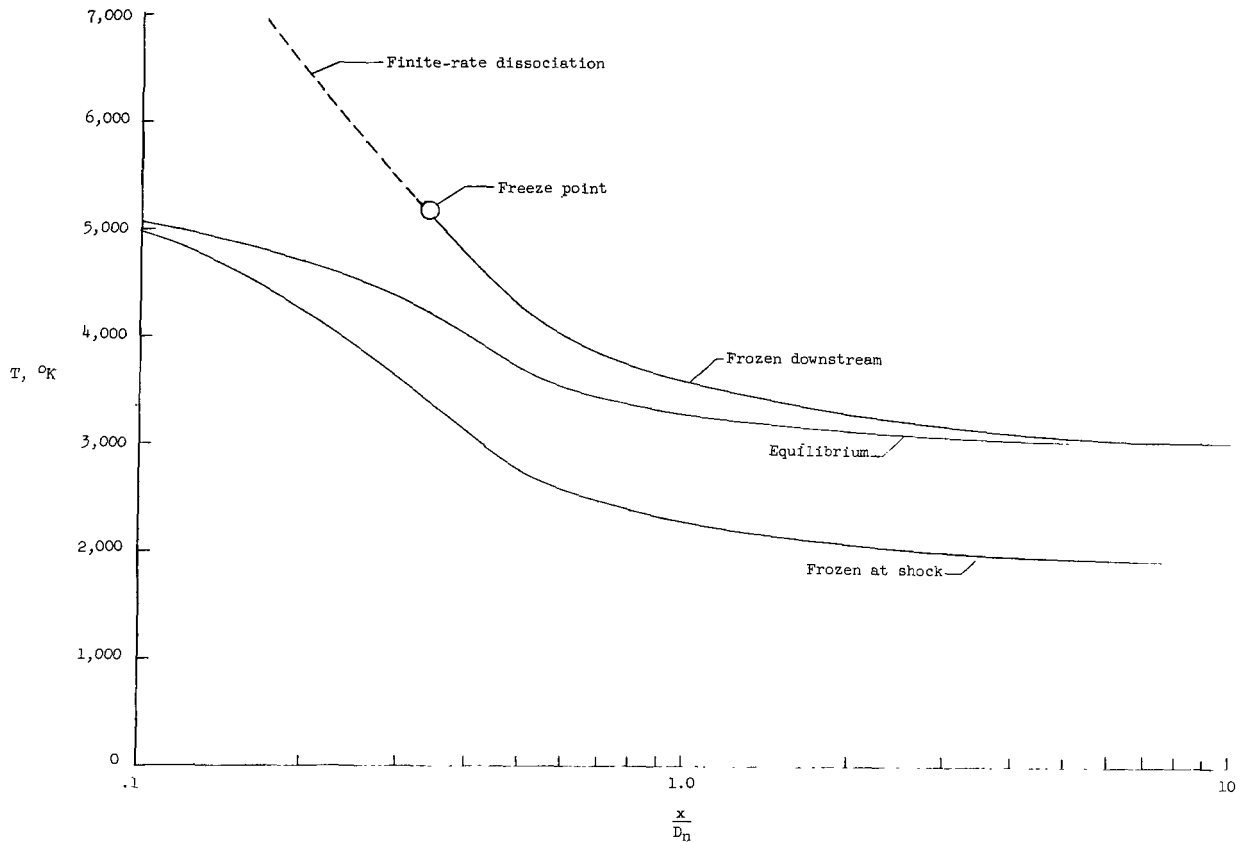


Figure 7.- Temperature distribution on streamline 1 for equilibrium, frozen at shock, and frozen downstream cases.

Second, assumptions were made about the ionic state of the air. The limiting conditions were: (1) complete ionic (as well as chemical) equilibrium throughout the flow, and (2) frozen ions (as well as chemistry) subsequent to the attainment of complete equilibrium in the shock front. Two intermediate calculations were made on the basis of frozen flow downstream of the freeze point. In one of these the reaction $N + O \rightleftharpoons NO^+ + e^-$ was considered to be in equilibrium at and downstream of the freeze point. In the other this reaction was assumed to be in equilibrium at the freeze point but downstream of this point a finite rate was used for the recombination of NO^+ and e^- .

Third, inviscid flow was assumed throughout the shock layer as a first approximation. Boundary-layer corrections were made only for the calculations in which complete equilibrium was assumed and for those in which finite-rate recombination of ions was assumed. Figure 8 shows the variation of electron concentration along a typical streamline for the following assumptions:

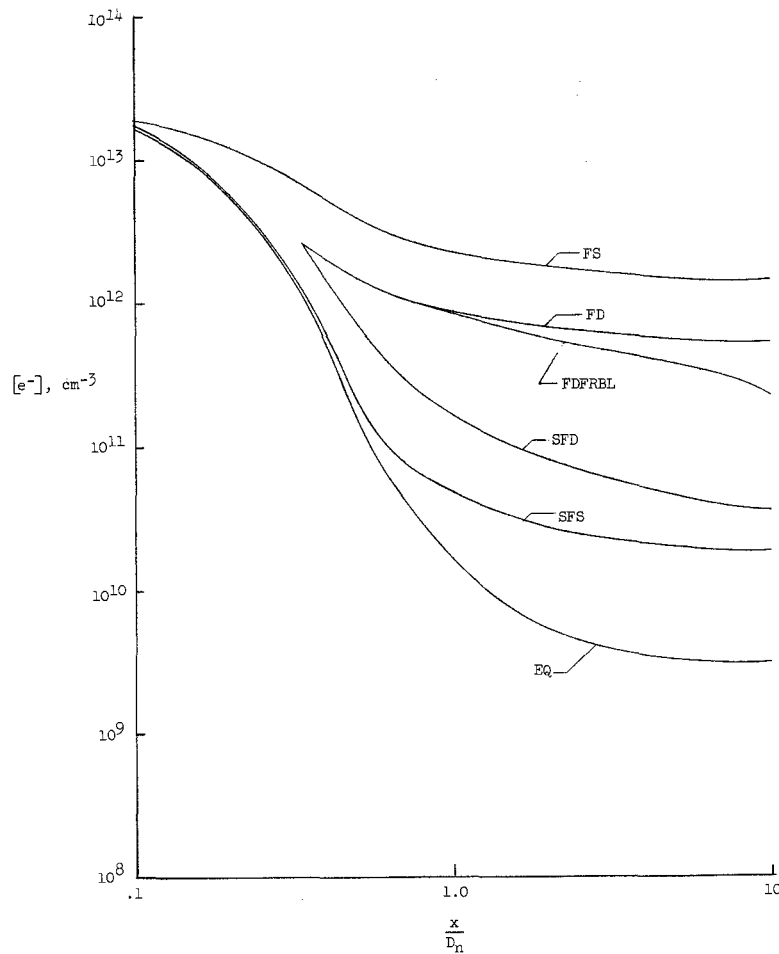


Figure 8.- Electron concentration along stream-line 1 for several chemical-ionic models.

- EQ equilibrium, complete thermal equilibrium throughout the flow
- FS frozen shock, complete freezing of composition at shock-front equilibrium values
- SFS semifrozen shock, same as FS but with $N + O \rightleftharpoons NO^+ + e^-$ in local equilibrium
- FD frozen downstream, same as FS except that freezing takes place downstream of shock and is not an equilibrium composition at the freeze point
- SFD semifrozen downstream, same as FD but with $N + O \rightleftharpoons NO^+ + e^-$ in local equilibrium
- FDFRBL frozen downstream with finite rate recombination of ions and with boundary-layer corrections, same as FD but with allowance for (1) a finite rate for $NO^+ + e^- \rightarrow N + O$ and (2) altered values of velocity, temperature, and density after the streamline enters the boundary layer

NONEQUILIBRIUM CONCEPTS

In general the true plasma properties are best represented by calculations which include the effects of finite reaction rates. The most accurate way to do this is to use a computer program which simultaneously calculates composition, thermodynamic properties, and flow-field properties. The following approximate treatment of nonequilibrium processes was satisfactory for the purposes of this study.

In this paper air is assumed to be a mixture of 21 percent oxygen and 79 percent nitrogen. The dissociation rate of initially undissociated air is controlled by the dissociation rate of O_2 , as can be seen from the calculations reported in references 17 and 18. A fairly accurate model for calculating the dissociation rate of air is therefore a dissociating diatomic gas for which the dissociation rate is identical to that of pure O_2 . However, because of the large difference between the dissociation energies of O_2 and N_2 , the thermodynamic properties of this gas are not accurately represented by dissociating O_2 . These thermodynamic properties were assumed to be identical to the properties of a dissociating mixture which is initially 21 percent O_2 and 79 percent N_2 and in which the ratio of O atom concentration to N atom concentration is fixed at 5 to 1 and rotation and vibration are in equilibrium. The choice of this particular ratio was based on figure 9 which shows $[O]/[N]$ as a function of $[O_2]$ behind a normal shock wave in air at shock temperatures comparable to the range of interest in this paper. (The curves in figure 9 are crossplots of figures 9 and 10 in reference 17.) The value of $[O]/[N]$ for the 10,000° K shock temperature approaches 5 to 1, but the 7,000° K data call for a value of $[O]/[N]$ of the order of 50 to 1. This factor-of-10 discrepancy is not as serious as it seems at first sight, since the degree of dissociation produced along the cooler streamlines is small.

The NO concentration was arbitrarily taken to be zero. This is equivalent to assuming that half the NO molecules are O_2 and the other half are N_2 . Since the specific heats of O_2 , NO, and N_2 are approximately the same, the most serious error involved is the neglect of the heat of formation of NO from O_2 and N_2 , which causes the temperature predicted by the model to be too low. For example, if the mole fraction of NO is 0.1 and $\alpha = 0.2$, then the temperature error due to this cause is of the order of 300° K.

The variation of the degree of dissociation along a streamline was calculated by graphical integration of a plot of $d\alpha/ds$ against s , where $d\alpha/ds$ is given by the equation

$$\frac{d\alpha}{ds} = 2.41 \times 10^{20} \left(\frac{k_d}{u} \right) \left(\frac{p}{T} \right) (0.25 - \alpha) \quad (1)$$

which is the first term in the expression for da/dt obtained from equation (10) of reference 19 with $(g - \alpha)(1 + \alpha)$ replaced by $(0.25 - \alpha)$ and with all the

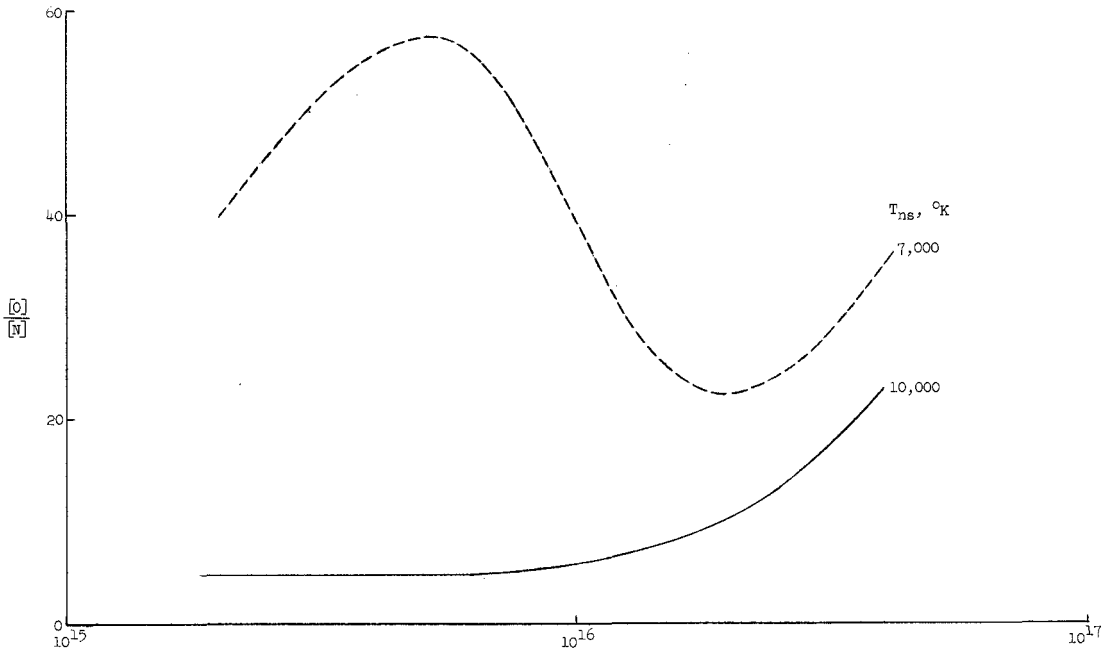


Figure 9.- Ratio of $[O]$ to $[N]$ as a function of $[O_2]$ behind a normal shock in air. (Data from ref. 17.)

multiplicative constants combined into one. The second term in the cited equation from reference 19 accounts for three-body recombination of atoms and is negligible at the air densities appropriate to the problem considered here. The dissociation rate k_d was taken from equation (13) of reference 19. The quantities u , p , T , and α were local streamline values.

As was mentioned previously, the pressure variation along a streamline was assumed to be identical to that calculated for equilibrium inviscid flow. The u and T variations were found by alternately expanding the gas at constant composition and dissociating it at constant pressure. This was done in small steps and the corresponding reaction path in the enthalpy-temperature plane was determined through the use of the equation of state and the conservation equations for mass, energy, and momentum. In order to perform these operations the α, s relation had to be specified.

In order to obtain a relation between α and s , equation (1) was integrated by means of an iteration procedure in which the output α, s relation was fed back into the procedure as an input. The initial α, s relation was assumed to be $\alpha = 0$ for all values of s . Fortunately, the process converged rapidly.

The reaction rate on the body streamline was such that equilibrium was attained in a distance of the order of the standoff distance of the shock from the nose. Recombination processes were so slow that the remainder of the body streamline was considered to be chemically frozen. Along most of the other streamlines chemical equilibrium was never attained; the rate simply slowed to

essentially zero because of the dropping temperature and density in the expanding flow. Downstream of the freeze point on the streamlines the chemical composition was assumed to be constant.

In order to obtain an estimate of the electron concentration at the freeze point, equilibrium was assumed for the $N + O \rightleftharpoons NO^+ + e^-$ reaction at the local temperature. The rate given for this reaction in reference 18 indicates that this should be a good approximation.

A calculation of the effect of error in $[O]/[N]$ on the equilibrium electron concentration revealed that, if $[O]/[N]$ should be 50 to 1 at the freeze point instead of 5 to 1, the electron concentration should be increased by a factor of $(10)^{1/2} = 3.16$. Also, underestimation of the freeze-point temperature by 300° K (which would be caused by neglecting the heat of formation of 10 percent NO in the mixture) would require that the electron concentration be increased by a factor of about 1.15 at $5,000^\circ$ K. Taken together these effects indicate that the electron concentration may be underestimated by a factor of about 3.6.

Finite-rate recombination of the electrons was assumed to be controlled by the dissociative recombination process $NO^+ + e^- \rightarrow N + O$ and was evaluated by integrating the equation

$$\frac{d}{dt}[e^-] = -k_r[NO^+][e^-] \quad (2)$$

along the streamlines. The rate k_r was taken from reference 18 and $[NO^+]$ was taken to be equal to $[e^-]$.

Frozen downstream values of velocity, temperature, and density were used until the streamlines entered the boundary layer. Boundary-layer values were used for the remaining portions.

BOUNDARY-LAYER TREATMENT

Boundary-layer corrections were applied only to the calculations in which complete equilibrium was assumed and to those in which finite-rate recombination of ions was assumed. Both calculations were made by using the similar solutions for laminar equilibrium boundary layers of reference 16 and then matching the resulting profiles to the inviscid flow to account grossly for vorticity interaction. Briefly, the procedure began with the calculation of velocity, temperature, and density profiles in the boundary layer at representative axial body stations. At each of these stations the flow properties at the edge of the boundary layer ($y = \delta$) were assumed to be the same as those at the body surface ($y = 0$) in the inviscid flow field.

The real-gas method of reference 16 was applied under the assumptions of equilibrium thermal properties, Lewis number of 1, and pressure gradient of 0.

Because of the last assumption, no stations closer to the stagnation point than $\frac{x}{D_n} = 0.4$ were used. Hence, for complete equilibrium the resulting boundary-layer properties should be closely determined by this method, if one excludes that aspect of the problem due to free-stream shear which must be treated crudely in any case.

For the frozen flow the same method was used, but the inviscid surface properties, which also are the boundary-layer edge properties, were determined from the frozen downstream flow field. The resulting boundary layer can be described as being in pseudoequilibrium, since the thermal and transport properties in reference 16 are for equilibrium air.

The flow properties used in the boundary-layer calculations at $y = 0$ and at $y = \delta$ are given for several body stations in table II. The viscous and inviscid profiles of velocity, temperature, and density at a given station were then merged by a matching procedure which favored boundary-layer values close to the body and inviscid flow values far from the body. The center of the transition region from inviscid to viscous flow solutions was arbitrarily selected to

TABLE II.- FLOW PROPERTIES AT BODY SURFACE AND AT EDGE OF BOUNDARY LAYER

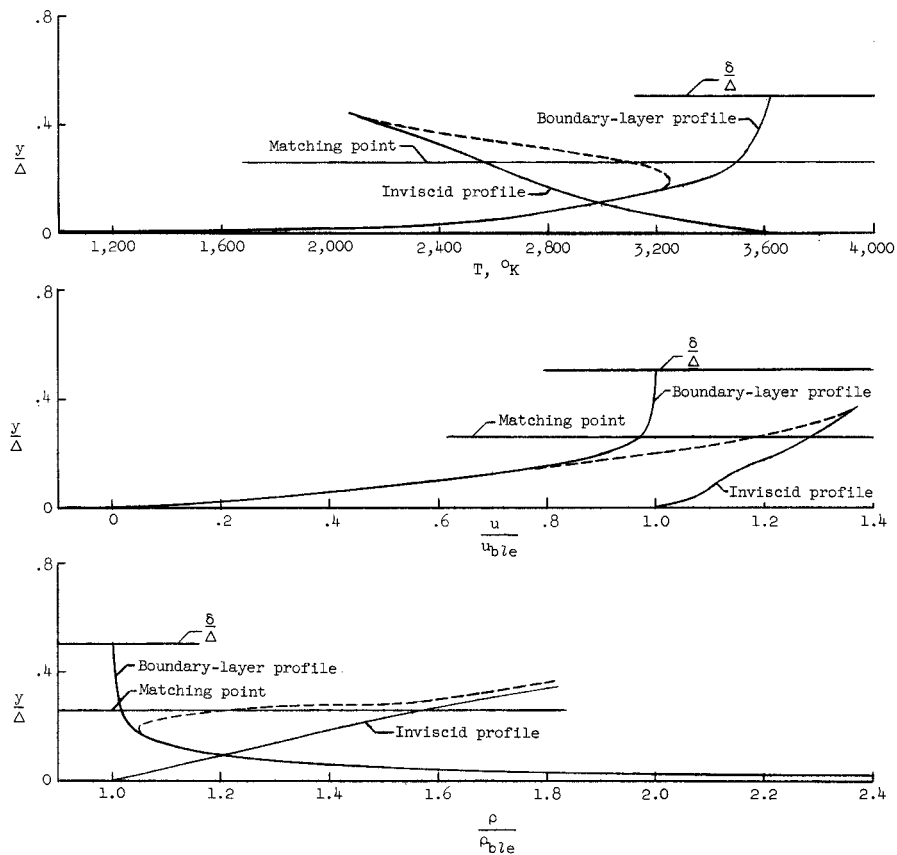
$\frac{x}{D_n}$	Equilibrium flow		Frozen flow	
	$y = 0$	$y = \delta$	$y = 0$	$y = \delta$
$u, \text{ft-sec}^{-1}$				
0.40	0	10,089	0	8,076
1.00	0	11,047	0	8,556
2.00	0	11,474	0	8,868
5.40	0	11,830	0	9,039
11.50	0	11,786	0	9,011
$T, ^\circ\text{K}$				
0.40	$400 < T < 800$	4,410	$400 < T < 800$	2,619
1.00	↓	4,040	↓	2,252
2.00	↓	3,830	↓	2,002
5.40	↓	3,630	↓	1,861
11.50	↓	3,660	↓	1,884
ρ/ρ_{s1}				
0.40	85.00×10^{-4}	8.67×10^{-4}	37.30×10^{-4}	12.60×10^{-4}
1.00	49.32	5.03	25.60	8.65
2.00	30.22	3.78	18.48	6.45
5.40	23.76	2.97	15.21	5.38
11.50	24.54	3.07	15.87	5.54

be that point (value of y) in the boundary-layer solution at which the velocity begins to drop off sharply from the value at the edge and is referred to herein as a matching point. In the neighborhood of this matching point the velocity, temperature, and density profiles were joined by a smooth fairing from the one to the other. Figure 10 illustrates the method and some typical profiles.

Streamlines were followed into the boundary layer by using a mass-flow parameter w to identify streamlines, where w is defined by the relation

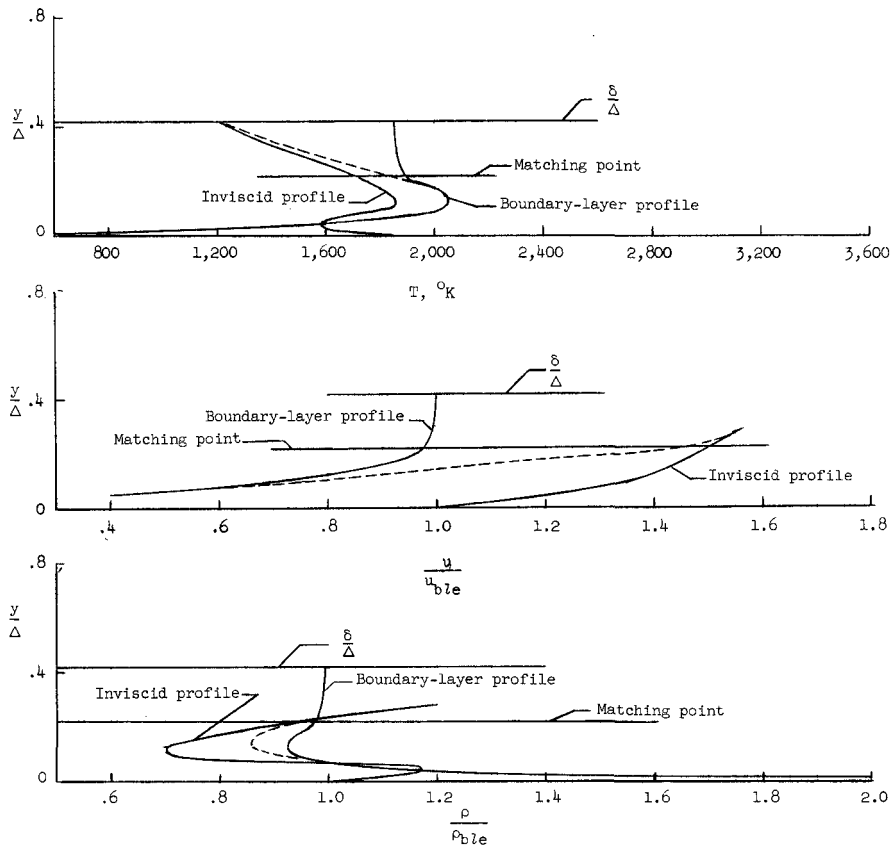
$$w(y) = 2\pi r \int_0^y \rho u \, dy$$

The concept is adopted that the mass flow interior to a surface of revolution generated by rotating a streamline about the body axis is the same at all axial locations on the body. The concept of flow streamlines as particle paths becomes invalid in the presence of diffusion, which should be present in a reacting boundary layer. However, in lieu of a more proper approach and recognizing that the



(a) Equilibrium flow. $\frac{x}{D_n} = 5.4$.

Figure 10.- Typical boundary-layer profiles.



(b) Frozen downstream flow. $\frac{x}{D_n} = 5.4$.

Figure 10.- Concluded.

results will be increasingly poor toward the body surface, "streamlines" were followed into the boundary layer by tracing the locus of constant w in the $x/D_n, y/\Delta$ plane. The streamlines found in this way are shown in figure 11.

CONSTRUCTION OF $[e^-]$ AND ν PROFILES

Shock-layer profiles of electron concentration and collision frequency were constructed at axial stations $\frac{x}{D_n} = 0.42, 1, 2, 5.4,$ and 11.5 . Representative samples of these profiles are shown in figures 12 and 13. These profiles are slightly different from the profiles given in references 12 and 13 for the same body and flight conditions. The changes represent improved knowledge of the $[e^-]$ and ν variations based on more detailed calculations which considered more streamlines than were used for the former calculations.

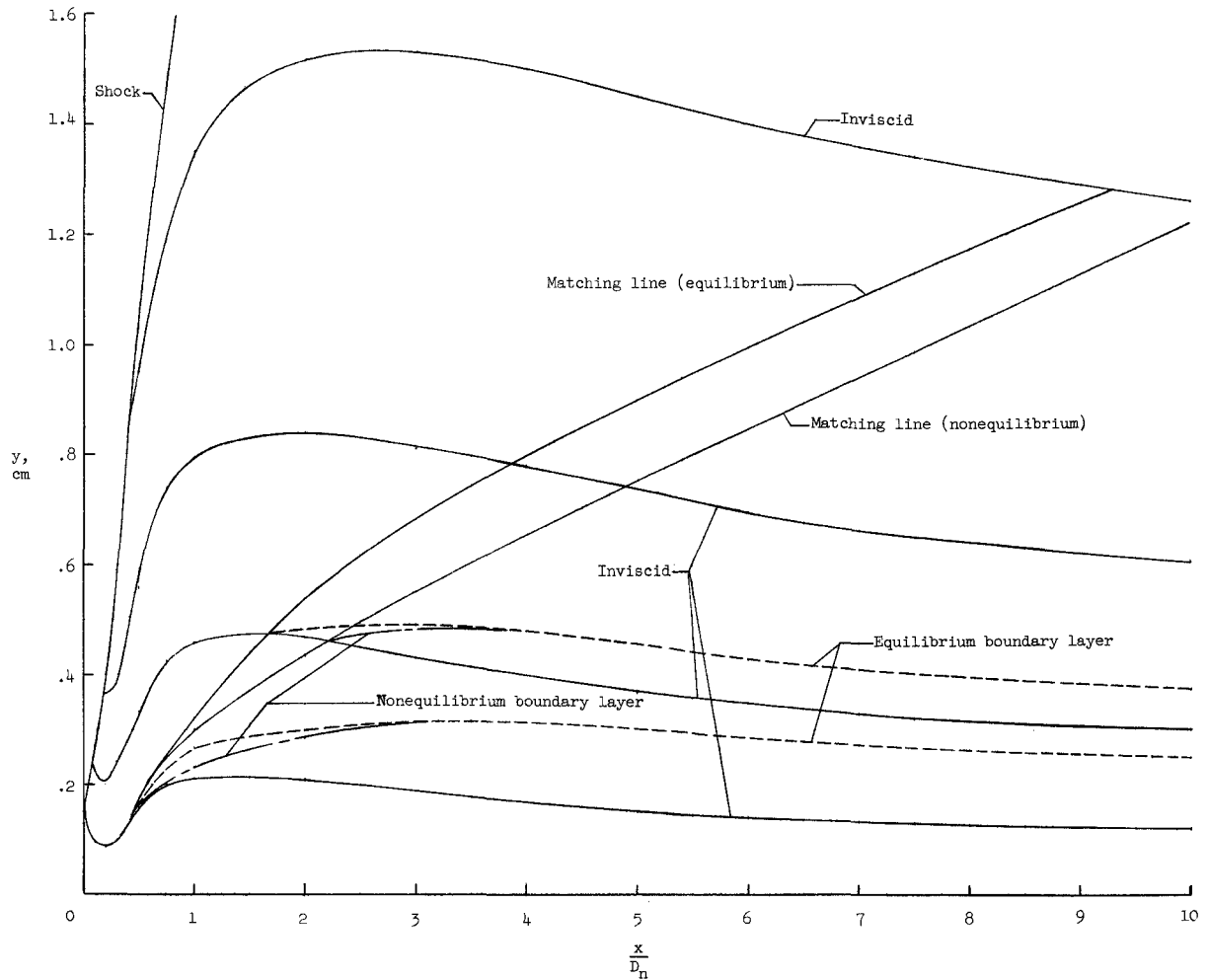


Figure 11.- Flow "streamline" paths in boundary-layer region.

Except for the two profiles involving boundary-layer corrections, the $[e^-]$ profiles are simply cross plots of streamline calculations like those shown in figure 8. For EQBL the EQ profile was modified in the boundary-layer region by calculating the equilibrium electron concentration corresponding to the local temperature and density in the boundary layer.

The reasoning for FDFRBL is a little more involved. As for the other profiles the process was begun by cross-plotting points from streamline calculations. In the boundary-layer region the properties along streamlines were corrected for boundary-layer effects. However, too few streamlines were calculated to define the sharp dropoff in the $[e^-]$ profiles which occurs close to the body surface and, in contrast to EQ, $[e^-]$ does not depend uniquely on local values of

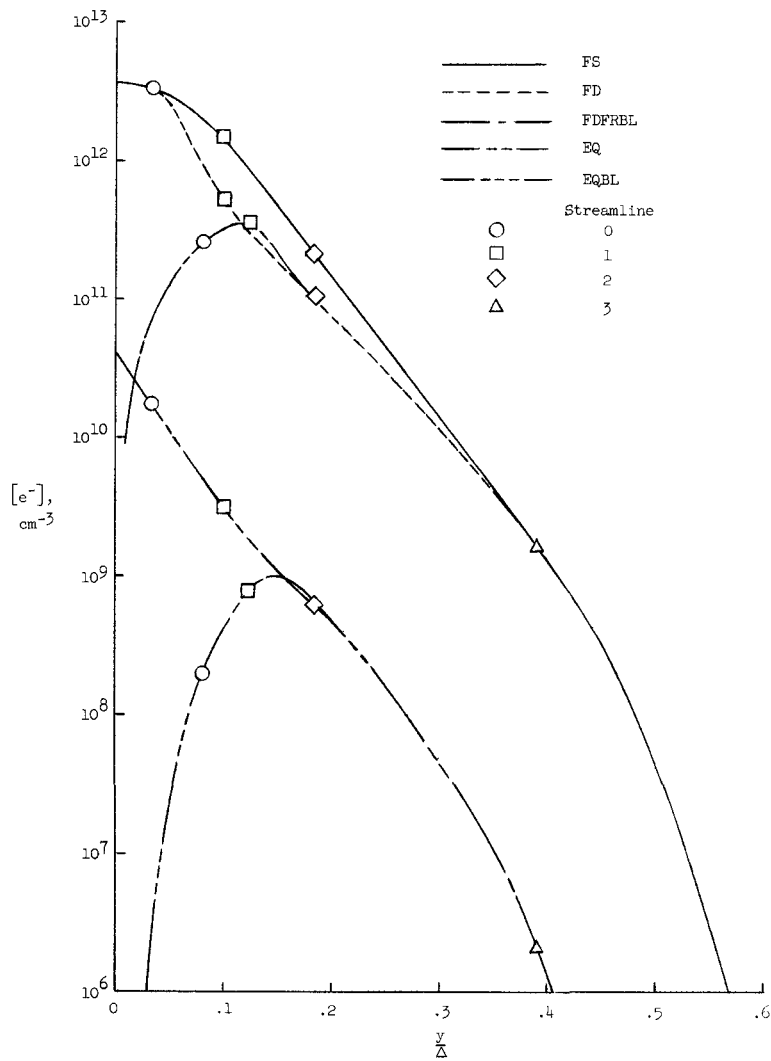


Figure 12.- Electron concentration profiles. $\frac{x}{D_n} = 5.4$.

temperature and density. Therefore, the transition through this part of the boundary layer was determined by the following procedure:

(1) Let equation (2) be expressed by the formula $\frac{d[e^-]}{dt} = -k_r [e^-]^2$, where k_r is a function of temperature only.

(2) Divide this equation by $u = \frac{ds}{dt}$ to obtain

$$\frac{d[e^-]}{ds} = -\frac{k_r [e^-]^2}{u} \quad (3)$$

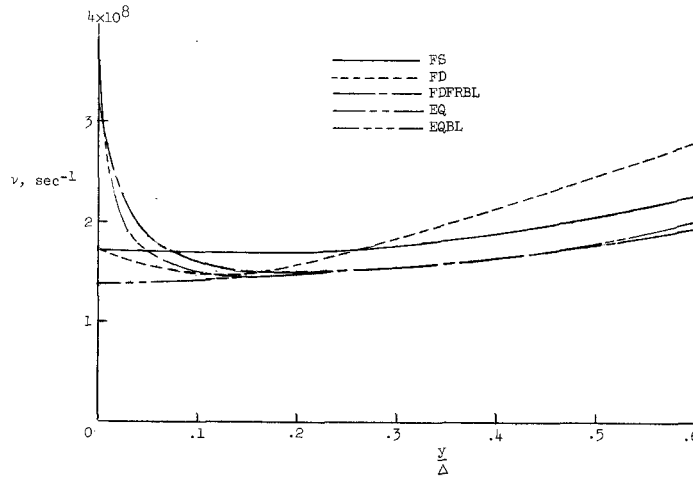


Figure 13.- Collision frequency profiles. $\frac{x}{D_n} = 5.4$.

(3) Choose a characteristic reaction distance based on the idea that, if the reaction rate were held constant, $[e^-]$ would vanish in unit distance. In equation form this is expressed as

$$\frac{d[e^-]}{ds} = -[e^-]_{\text{initial}}$$

The definition of the characteristic reaction distance is arbitrary. Its purpose is to establish an order of magnitude value of $\frac{d[e^-]}{ds}$ which would be able to cause appreciable decay of the electron concentration in the flow time over the body.

(4) Then, if the ratio of k_r to u is held constant in equation (3), the rate at which electrons disappear decreases very quickly as $[e^-]$ becomes smaller. For example, a decrease in $[e^-]$ by a factor of 10 would cause the local characteristic reaction distance to increase by a factor of 100. Thus, $[e^-]$ has a strong dependence on the local value of k_r/u . Reaction equations with this behavior are described as "self-limiting." It should be noted that, except for the dependence on k_r/u , $\frac{d[e^-]}{dt}$ depends only on the magnitude of the electron concentration. Thus, for comparable values of k_r/u , the electron concentration is about the same in any flow field in which electron recombination is taking place according to equation (3).

(5) As a result, the following equations are based on the idea of maintaining a local characteristic reaction distance of 1 foot:

$$\frac{1}{-[e^-]} \frac{d[e^-]}{ds} = \frac{k_r}{u} [e^-] = 1$$

or

$$[e^-] = \frac{u}{k_r} \quad (4)$$

Electron concentration profiles defined by equation (4) approach zero at the wall, vary in a reasonable way through the boundary layer, and come close to joining smoothly onto profiles determined from streamline calculations. Exact junctions are obtained by applying constant multipliers to values of $[e^-]$ obtained from equation (4). The section of the FDFRBL curve in figure 12 between $y = 0$ and the point corresponding to streamline 0 was obtained in this way. Note that this section of the profile is independent of any reasonable choice for the characteristic reaction distance, since the shape is uniquely determined by the variation of u/k_r , and the arbitrary multiplier compensates for different choices of the characteristic length.

The collision frequency was evaluated from the relation

$$\nu = 1.6 \times 10^{12} \frac{p}{\sqrt{T}} = 4.52 \times 10^{27} \frac{\bar{Q}p}{\sqrt{T}}$$

and typical results are shown in figure 13. This expression is based on the assumption of a constant velocity-averaged effective collision cross section of $\bar{Q} = 3.54 \times 10^{-16} \text{ cm}^2$. The value of \bar{Q} is based on the electron-molecule cross sections for O_2 and N_2 given in reference 20 (p. 206) and on the electron-atom cross section for O given in reference 21. (The cross sections for N and O were assumed to be the same.)

CALCULATION OF TRANSMITTED AND REFLECTED SIGNAL STRENGTH

The propagation problem was assumed to be equivalent to the calculation of the energy transmitted and reflected by a plane-parallel slab of plasma in which $[e^-]$ and ν vary only in the propagation direction. Monochromatic plane waves at normal incidence impinge on one side of the slab. Reference 12 shows that this problem reduces to the solution of the differential equation

$$\frac{d^2 E}{dy^2} + k^2 E = 0 \quad (5)$$

where E is the complex electric vector, y is distance measured in the propagation direction from the plasma boundary on the incidence side, and k is the complex wave number.

A number of assumptions are implicit in this formulation of the problem. Among these are: (1) the plasma properties are not affected by the electromagnetic radiation, (2) detuning of the antenna in the presence of plasma is neglected, (3) variations of the plasma properties in directions perpendicular to the propagation direction are neglected, (4) curvature of the plasma is ignored, and (5) the boundary condition at the body surface may not be realistic.

The plane slab model was used because it led to tractable solutions of the propagation equations. Because of the plane wave assumption, calculated values of signal attenuation are more likely to be correct for an X-band open waveguide antenna than for a slot antenna operating in the VHF range, such as the one on the RAM A1 vehicle. However, there is no restriction on the steepness of plasma gradients in the nonhomogeneous layer.

The solution of equation (5) subject to appropriate boundary conditions was carried out by machine integration by using the Runge-Kutta procedure. Equation (5) was reduced to the following set of simultaneous differential equations in real variables:

$$\frac{d^2 f}{dy^2} + k_0^2 (fV - gW) = 0$$

$$\frac{d^2 g}{dy^2} + k_0^2 (fW + gV) = 0$$

where

$$E = f + ig$$

$$k^2 = k_0^2 (V + iW) = (\alpha + i\beta)^2$$

$$V = 1 - \frac{1}{\left(\frac{v}{\omega_p}\right)^2 + \left(\frac{\omega}{\omega_p}\right)^2}$$

$$W = \frac{v/\omega_p}{\omega/\omega_p} \frac{1}{\left(\frac{v}{\omega_p}\right)^2 + \left(\frac{\omega}{\omega_p}\right)^2}$$

The symbols k_0 , α , β , v , ω , and ω_p have their customary meanings in equations of this kind. The phase parameter α and the attenuation parameter β are related to V and W as follows:

$$\alpha = \frac{k_0}{\sqrt{2}} \left[V + \sqrt{V^2 + W^2} \right]^{1/2}$$

$$\beta = \frac{k_0}{\sqrt{2}} \left[-V + \sqrt{V^2 + W^2} \right]^{1/2}$$

Figure 14 shows a typical variation of V and W through a plasma layer. Continuity of V and W at the boundaries is not required and will not be present if $[e^-]$ is discontinuous at the boundaries. In this figure the incident wave is indicated by the unit amplitude plane wave $e^{ik_0 y}$. The reflected and transmitted waves are also indicated as plane waves with the complex amplitudes E_R and E_T , respectively.

The values of V and W in mediums 0 and 2 are taken to be equal to the values in vacuum. The waves are assumed to be simple harmonic in time with frequency ω .

Continuity of E and E' at the boundaries requires that the following relations be satisfied:

$$E_{0a} = 1 + |E_R| e^{i\phi_a} = E_{1a} \quad (6)$$

$$E'_{0a} = ik_0 - ik_0 |E_R| e^{i\phi_a} = E'_{1a} \quad (7)$$

$$E_{1b} = |E_T| e^{i(k_0 \Delta + \phi_b)} = E_{2b} \quad (8)$$

$$E'_{1b} = ik_0 |E_T| e^{i(k_0 \Delta + \phi_b)} = E'_{2b} \quad (9)$$

The propagation equations cannot be numerically integrated in the propagation direction because E_R is unknown. The integration can be performed in the

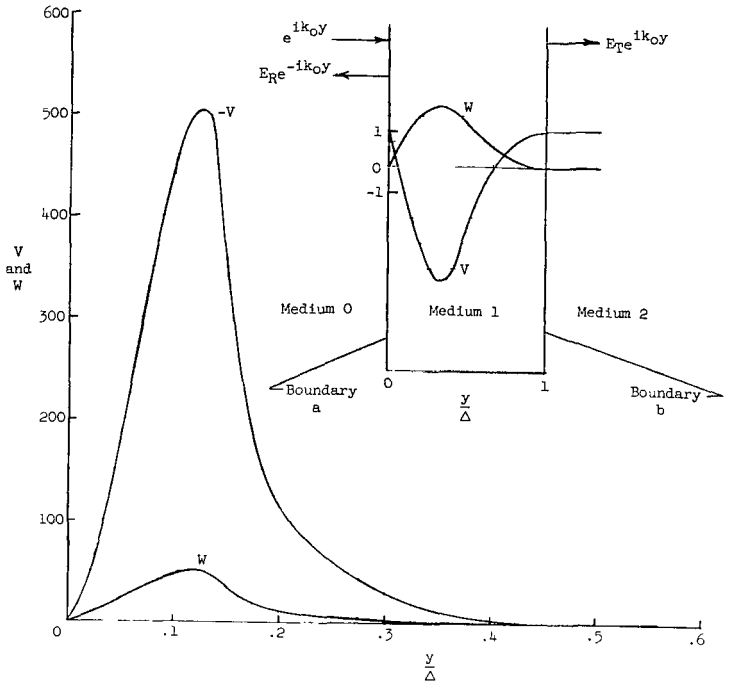


Figure 14.- Variation of V and W in the shock layer. FDFRBL; $\frac{x}{D_n} = 5.4$.

opposite direction, however, if the equations for the boundary conditions are divided by $|E_T| e^{i(k_0 \Delta + \phi_b)}$, as follows:

$$\bar{E}_{0a} = I + \bar{E}_R e^{i\phi_a} = \bar{E}_{1a}$$

$$\bar{E}'_{0a} = ik_0 I - ik_0 \bar{E}_R e^{i\phi_a} = \bar{E}'_{1a}$$

$$\bar{E}_{1b} = 1 = \bar{E}_{2b}$$

$$\bar{E}'_{1b} = ik_0 = \bar{E}'_{2b}$$

where

$$I = \frac{e^{-i(k_0 \Delta + \phi_b)}}{|E_T|}$$

$$\bar{E}_R = \frac{|E_R| e^{-i(k_0 \Delta + \phi_b)}}{|E_T|}$$

The quantities needed for the calculation of the transmitted and reflected signal strength are $|E_T|$ and $|E_R|$ from equations (6) to (9). These are related to $|I|$ and $|\bar{E}_R|$ as follows:

$$|E_T| = \frac{1}{|I|}$$

$$|E_R| = \frac{|\bar{E}_R|}{|I|}$$

The integration was begun at $y = \Delta$ where $\bar{f} = 1$, $\bar{f}' = 0$, $\bar{g} = 0$, $\bar{g}' = k_0$, and was continued to $y = 0$ to find the values of \bar{f} , \bar{f}' , \bar{g} , and \bar{g}' at $y = 0$. These values were then substituted in the following formulas to find $|I|$ and $|\bar{E}_R|$:

$$|I| = \frac{1}{2k_0} \sqrt{(k_0 \bar{f} + \bar{g}')^2 + (k_0 \bar{g} - \bar{f}')^2}$$

$$|\bar{E}_R| = \frac{1}{2k_0} \sqrt{(k_0 \bar{f} - \bar{g}')^2 + (k_0 \bar{g} + \bar{f}')^2}$$

The final results on reflected and transmitted signal strength were obtained in terms of signal power loss in decibels. The transmission loss due to reflection from the plasma is

$$(SL)_R = 10 \log(1 - |E_R|^2)$$

The transmission loss due to both reflection and attenuation is

$$(SL)_t = 20 \log|E_T|$$

The calculated transmission loss for various flow assumptions is given in figure 15. The ratio of reflection loss to loss caused by both reflection and attenuation is given in figure 16.

The normal incidence program described has been generalized to cover plane waves incident at any angle on a nonhomogeneous slab. The new program was reported in reference 12 and was applied to a study of plasma reciprocity (interchange of incidence and transmission sides of the plasma) in reference 22.

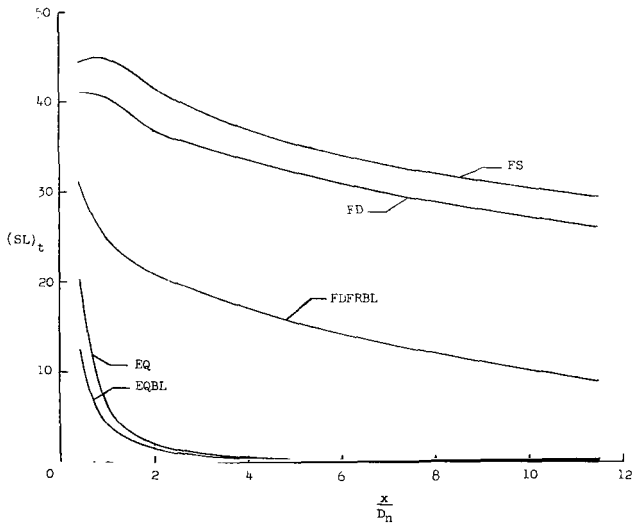


Figure 15.- Signal loss as a function of axial distance from the nose.

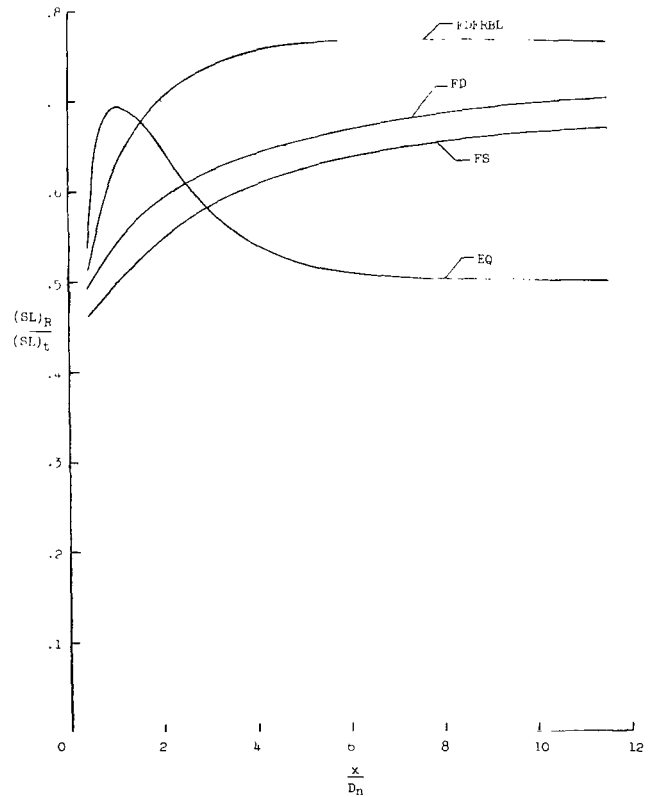


Figure 16.- Fraction of signal lost by reflection.

CONCLUDING REMARKS

Even on the basis of the crude models used in this study, the indication is clear that adequate description of plasma properties for the purpose of calculating radio signal attenuation will in general require that allowance be made for (1) finite rate chemistry and ionization and (2) the presence of a boundary layer.

The plane slab model used for calculation of signal attenuation is more likely to give good results when the signal wavelength is small compared to body dimensions, which was not the case for the VHF slot antenna on RAM A1. Thus, the numerical values of signal attenuation given herein are questionable and should be recalculated as soon as a program is available which is based on a geometry more closely approximating the actual case. Other areas in which improvements might be made are consideration of antenna-plasma interactions and proper definition of boundary conditions at the boundary near the antenna.

Langley Research Center,
National Aeronautics and Space Administration,
Langley Station, Hampton, Va., September 10, 1963.

REFERENCES

1. Rotman, Walter, and Meltz, Gerald, eds.: Electromagnetic Effects of Re-Entry. Planetary and Space Sci., vol. 6, June 1961.
2. Sims, Theo E., and Jones, Robert F.: Flight Measurements of VHF Signal Attenuation and Antenna Impedance for the RAM Al Slender Probe at Velocities up to 17,800 Feet Per Second. NASA TM X-760, 1963.
3. FitzGibbon, Sheila A.: Real Gas Supersonic Flow Field Solutions in the Shock Layer Around a 90° Sphere-Cone at Mach = 20.4, 21.4, and 21.2. Aerod. Data Memo No. 1:48, Missile and Space Vehicle Dept., Gen. Elec. Co., May 1961.
4. Lin, S. C., and Teare, J. D.: A Streamtube Approximation for Calculation of Reaction Rates in the Inviscid Flow Field of Hypersonic Objects. Res. Note 223(AFBSD-TN-61-24), Avco-Everett Res. Lab., Aug. 1961.
5. Kennedy, E., and Fields, A.: The Numerical Calculation of the Flow Field Around a Reentry Body. Tech. Rep. 231 (Contract AF 19(604)-7400 to M.I.T. Lincoln Lab.), Gen. Appl. Sci. Labs., Inc., Apr. 24, 1961. (Reissued Sept. 18, 1962.)
6. Eschenroeder, Alan Q.: Ionization Nonequilibrium in Expanding Flows. ARS Jour., vol. 32, no. 2, Feb. 1962, pp. 196-203.
7. Blottner, F. G., and Mathieu, R. D.: The Calculation of a Chemically Reacting Boundary Layer Flow Along a Body. Doc. No. 62SD618 (Contract AF 04(647)-617), Re-Entry Syst. Dept., Gen. Elec. Co., Sept. 25, 1962.
8. VanTassell, William, and Pallone, Adrian: Similar Solutions of the Compressible Laminar Boundary-Layer Equations for Air in Equilibrium Dissociation and Ionization With and Without Air Injection in the Stagnation Region. RAD-IM-61-22 (Contract AF 04(647)-305), AVCO Res. and Advanced Dev. Div., June 28, 1961. (Available from ASTIA as AD 259 707.)
9. Galwin, Lawrence S.: Integral Method Solution for a Dissociated Laminar Boundary Layer Applied to a Hypersonic Reentry Body. Tech. Rep. No. 313 (Contract No. DA-30-069-ORD-3531), Gen. Appl. Sci. Labs., Inc., Sept. 5, 1962.
10. Klein, M. M., Greyber, H. D., King, J. I. F., and Brueckner, K. A.: Interaction of a Non-Uniform Plasma With Microwave Radiation. Planetary and Space Sci., vol. 6, 1961, pp. 105-115.
11. Graf, K. A., and Bachynski, M. P.: Existing Solutions for Interaction of Electromagnetic Waves With Plasma of Simple Geometries. DAMP Tech. Monograph No. 62-07 (Contract DA 36-034-ORD-3144RD), Radio Corp. of America, June 1962.

12. Swift, Calvin T., and Evans, John S.: Generalized Treatment of Plane Electromagnetic Waves Passing Through an Isotropic Inhomogeneous Plasma Slab at Arbitrary Angles of Incidence. NASA TR R-172, 1963. ✓
13. Huber, Paul W., and Evans, John S.: Theoretical Shock-Layer Plasma Flow Properties for the Slender Probe and Comparison With the Flight Results. NASA paper presented at Second Symposium on the Plasma Sheath (Boston), Apr. 10-12, 1962.
- ✓ 14. Richmond, J. H.: Transmission Through Inhomogeneous Plane Layers. IRE Trans. on Antennas and Propagation, vol. AP-10, no. 3, May 1962, pp. 300-305.
15. Huber, Paul W.: Hypersonic Shock-Heated Flow Parameters for Velocities to 46,000 Feet Per Second and Altitudes to 323,000 Feet. NASA TR R-163, 1963. ←
16. Cohen, Nathaniel B.: Boundary-Layer Similar Solutions and Correlation Equations for Laminar Heat-Transfer Distribution in Equilibrium Air at Velocities up to 41,100 Feet Per Second. NASA TR R-118, 1961.
17. Duff, Russell E., and Davidson, Norman: Calculation of Reaction Profiles Behind Steady State Shock Waves. II. The Dissociation of Air. Jour. Chem. Phys., vol. 31, no. 4, Oct. 1959, pp. 1018-1027.
18. Lin, Shao-Chi, and Teare, J. Derek: Rate of Ionization Behind Shock Waves in Air. II. Theoretical Interpretations. The Physics of Fluids, vol. 6, no. 3, Mar. 1963, pp. 355-375.
19. Schexnayder, Charles J., Jr., and Evans, John S.: Measurements of the Dissociation Rate of Molecular Oxygen. NASA TR R-108, 1961.
20. Massey, H. S. W., and Burhop, E. H. S.: Electronic and Ionic Impact Phenomena. The Clarendon Press (Oxford), 1952. (Reprinted 1956.)
21. Lin, S. C., and Kivel, B.: Slow-Electron Scattering by Atomic Oxygen. Phys. Rev., Second ser., vol. 114, no. 4, May 15, 1959, pp. 1026-1027.
22. Swift, C. T.: A Reciprocity Theorem for the Interaction of Electromagnetic Plane Waves With a One-Dimensional Inhomogeneous Slab. Proc. IEEE (Correspondence), vol. 51, no. 9, Sept. 1963, pp. 1268-1269.